Materials & Design 130 (2017) 59–68

Contents lists available at ScienceDirect

Materials & Design

journal homepage: www.elsevier.com/locate/matdes

Numerical investigation of the influence of process conditions on the temperature variation in fused deposition modeling

Jie Zhang[a], Xin Zhou Wang[a], Wang Wang Yu[a,b], Yu He Deng[a,c,*]

[a] College of Materials Science and Engineering, Nanjing Forestry University, Nanjing 210037, China
[b] School of Mechanical Engineering, Nanjing Vocational Institute of Industry Technology, Nanjing 210023, China
[c] Key Laboratory of Wood Science and Technology Zhejiang Province, Lin'an 311300, China

ARTICLE INFO

Keywords:
Fused deposition modeling
Cooling rate
Mathematical model
Temperature field
Temperature gradient

ABSTRACT

An adaptable three-dimensional transient mathematical model of temperature variation with respect to space and time, during and after the fused deposition modeling (FDM), is proposed and applied with a boundary-adjusting finite difference method. This model enables researchers to study the influence of almost all other parameters on the temperature field and gradient variation when constructing any cuboid at fixed raster angle of 0(90)° and filling ratio of 100%. Some predicted but significant conclusions are reached: reheating of a deposited raster by a newly deposited one is universal and happens mainly in the layer thickness direction; temperature settings are the primary and direct factors determining temperature field variation, while layer thickness and printing speed can still exert their own influence; printing speed is predicted to be positively correlated to mechanical properties of FDM constructed components through the mechanism of thermal coalescence; strict energy management is required if a FDM printer of higher resolution is to be invented and applied. The technique of such mathematical model can provide immediate insights in the understanding of FDM process from the perspective of energy balance, many of which have never been revealed from previous reports yet.

GRAPHICAL ABSTRACT

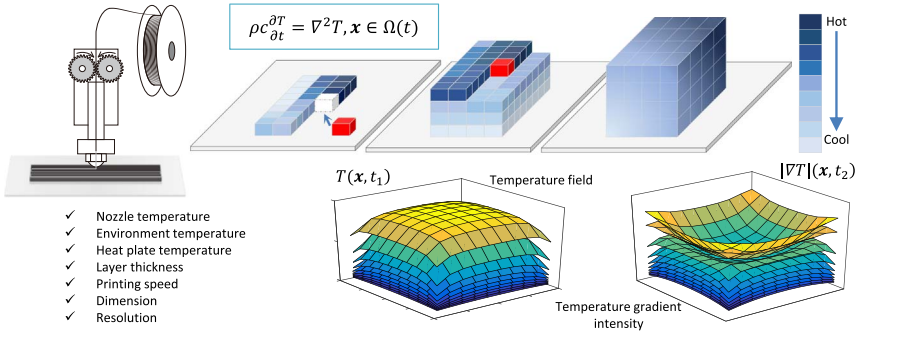

1. Introduction

Fused deposition modeling (FDM) is most commonly known as one process in which thermoplastic polymer is melted, extruded and deposited according to a prescribed pattern, in an additive manner, and under the control of certain program. Despite increased attention from the academy, industry and government in recent years, there are still a few fundamental questions regarding FDM like the crucial requirements on the properties of the material and the theoretical resolution limit for a FDM printer await to be answered. In essence,

* Corresponding author at: College of Materials Science and Engineering, Nanjing Forestry University, Nanjing 210037, China.
E-mail address: dengyuhe@hotmail.com (Y.H. Deng).

http://dx.doi.org/10.1016/j.matdes.2017.05.040
Received 22 March 2017; Received in revised form 11 May 2017; Accepted 12 May 2017
Available online 13 May 2017

these questions reflect the nature of FDM to be a controlled manufacturing process in an additive manner, characterizing energy balance and phase transition of the material. In seeking the nature of FDM, for example, researchers have extended the scope of material applicable in FDM from thermoplastic polymer to polymer blend [1,2], polymer based composite [3,4] and metal alloy of low melting point [5,6]. But current researches on FDM are mainly confined to experimental investigations of significant phenomena and overall parametric optimization [7–10]. There is a long way to reach a complete conception of FDM, understanding of which is a prerequisite before this rapid prototyping and additive manufacturing technique could be applied in wider areas with better performance.

Temperature management is a primary concern in FDM, as it has direct influence on the inter-layer bonding strength [11,12], rheological behavior [3,13], crystallinity of the polymer [14], deformation of the component [15,16], …, and indirect influence on macro mechanical properties, surface quality, printability, etc. Direct temperature measurement was attempted, but experimental results remain limited to date [11,17–19]. Sun and coworkers [11,19] had early attempts in temperature measurement in the bottom layer of the component constructed by FDM, using thermocouples of diameter down to 0.0118 mm. The influence of printing nozzle temperature, environment temperature, layer thickness, building orientation and geometry on temperature profile was discussed so as to correlate the parametric settings with the quality of bond formation. More recently, Kousiatza and Karalekas [18] reported utilization of fiber Bragg grating sensor and thermocouples to investigate local temperature variation with respect to time, but the measurable range of temperature was restricted to be below or close to the temperature of glass transition of the polymer. The difficulty of direct measurement lies in the characteristic dimension of FDM (200 μm, taking layer thickness) and the dimension of traditional thermocouple are comparable, and the measurement must be conducted in the three-dimensional dynamic building process of FDM, which is too demanding or even impossible for traditional measurement devices.

Analytical and/or numerical investigation is an alternative to provide insights in temperature variation with respect to space and time. There are some results available [12,16,20–24], among which, the research by Thomas and Rodríguez [12] is inspiring. They conducted a two dimensional (layer thickness and raster width) transient analytical of raster width-averaged temperature history at the interface, in a further attempt to model the inter-layer fracture strength from the perspective of wetting and diffusion bonding. Zhang and Chou [16] later employed an applicable finite element model, using element activation technique, to calculate the temperature variation in FDM; the research was designed to explain thermo-mechanical distortion through residual stress distribution, but only considered the influence of tool-path pattern on temperature variation. More recently, Costa and coworkers [20,24] conducted comprehensive parametric studies of temperature profile of single raster in FDM, with an emphasize on the reheating and adhesion between rasters. To conclude without loss of generality, the geometry and the building process considered in all available researches, although comprehensive and significant with different respects, cannot yet cover featured process of additive manufacturing in FDM. Temperature variation, especially the variation of temperature field and related temperature gradient subjected to different process conditions, stills awaits to be modeled with a more adaptable model.

This paper presents such an adaptable model to simulate the influence of process conditions on the temperature variation in FDM with a boundary-adjusting finite difference method. A three-dimensional transient numerical model describing the real building up process of any cuboid by a FDM printer in the case of raster angle of 0(90)°, and filling ratio of 100% is presented. The influence of nozzle temperature, heat plate temperature, environment temperature, layer thickness, printing speed, geometry dimension and the resolution of FDM printer on the temperature field and gradient variation with respect to space and time is modeled and discussed with significant phenomena and inspiring cases. Numerical results are verified with comparison between significant phenomena and all available reported analytical/experimental results. Qualitative conclusions drawn make perfect logical sense and quantitative results remain informative and instructive. These results could be immediately applied in the research of bond formation, thermo-deformation, and many other researches on and applications of FDM.

2. Modeling and solution

2.1. Hypothesis and settings

2.1.1. Hypothesis

Four hypothesis regarding the physics in FDM are assumed in order to build up an applicable mathematical model to solve the problem of temperature variation with respect to time and space.

1. The influence of polymer crystallization on energy balance is insignificant.
2. The influence of heat radiation on temperature variation is neglected.
3. Thermal expansion and friction in micro viscous flow on energy balance is neglected.
4. The interior of FDM constructed component is pore-free in the case of filling ratio of 100%, and no contact heat resistance exists in heat conduction.

2.1.2. Settings of FDM printer

Some basic settings irrelevant to physical phenomena are necessary and listed below. For the sake of modeling, this paper will take poly (lactic acid) (PLA) as the feedstock used in FDM.

1. Raster angle is set at 0(90)° with a filling ratio of 100% (no air gap);
2. The model to be built is a cuboid of dimension $L = 4$ mm, $W = 4$ mm, $H = 2$ mm;
3. Printing speed of nozzle $v = 40$ mm/s;
4. Initial temperature of PLA upon deposition is equal to the temperature of printing nozzle, which is set at $T_n = 210^{\circ}C$;
5. Temperature of the supporting heat plate is held constant and near the glass transition temperature of PLA, $T_p = 60^{\circ}C \approx T_g$;
6. Temperature of the air is held constant, $T_a = 20^{\circ}C$;
7. Layer thickness is set at 200 μm;
8. Diameter of printing nozzle is 400 μm.

The model to be built up is adaptable when all the other settings, except the raster angle and filling ratio, are subjected to variation, assuming no mechanical or rheological setbacks. Unless specified otherwise, all parameters in different simulations in the following sections take default value listed above.

2.2. Modeling

2.2.1. Geometry

Given the basic settings, printing nozzle moves line by line, layer by layer, as depicted in Fig. 1(a). Taking a distance of Δx along the length direction of a single thread of deposited raster inside the component, a sub-milli-metrical scale cuboid is constructed of dimension $\Delta x \times \Delta y \times \Delta z$, in which, Δy, representing raster width, is equal to nozzle diameter $\Delta y = 400$ μm, and z, representing raster height, is equal to layer thickness $\Delta z = 200$ μm. This sub-milli-metrical cuboid is referred to as 'element' throughout. The number of such element in the length, width and height direction in the component is $N_L = \frac{L}{\Delta x}$, $N_W = \frac{W}{\Delta y}$, and $N_H = \frac{H}{\Delta z}$, respectively. Total number of element adds up to.

$$N = N_L \times N_W \times N_H.$$

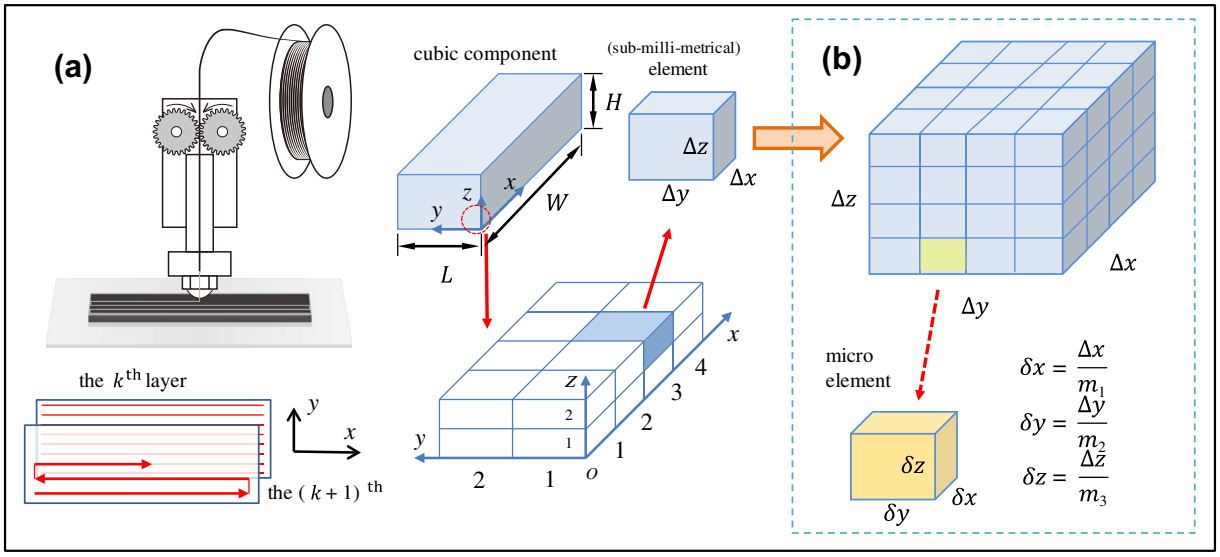

Fig. 1. (a) Geometry of FDM component and its sub-milli-metrical elements representation; (b) a multi-scale modeling strategy.

A time interval Δt is determined as the time required for the printing nozzle to move such a distance Δx, which is also the time required to deposit a single element,

$$\Delta t = \frac{\Delta x}{v}.$$

FDM process could thus be viewed as successive and chronological deposition of elements following a prescribed pattern at time intervals of Δt. The n^{th} element deposited at time $t(n) = t_n = n\Delta t$ is labeled as P_n or $P_{i,j,k}$, in which, $n = 1, 2, \cdots$, and (i,j,k) are integer spatial indices showing the position of this element inside the component (Fig. 1(a)) such $1 \le i \le N_L$, $1 \le j \le N_W$ and $1 \le k \le N_H$. $P_{i,j,k}$ also denotes the space occupied by the element. The temperature of element $P_{i,j,k}$ at t_n is assumed uniform and taken as $T^n_{i,j,k}$. Given the raster angle of 0(90)°, there is a bijective function between n and (i,j,k),

$$n(i,j,k) = \begin{cases} i + N_L \times (j-1) + N_L \times N_W \times (k-1), & j \text{ odd} \\ (N_L + 1 - i) + N_L \times (j-1) + N_L \times N_W \times (k-1), & j \text{ even} \end{cases}, \tag{1}$$

and conversely,

$$\begin{cases} k(n) = \frac{n - [\mathrm{mod}(n-1, N_L \times N_W) + 1]}{N_L \times N_W} + 1, \\ I(n) = \mathrm{mod}(n - (k-1)N_L \times N_W - 1, N_L) + 1, \\ j(n) = \frac{[n - (k-1)N_L \times N_W] - I}{N_L} + 1, \\ i(n) = \begin{cases} I, & j \text{ odd} \\ N_L + 1 - I, & j \text{ even} \end{cases} \end{cases}. \tag{1$_*$}$$

Temperature of all chronologically deposited elements at time t_n is denoted as a column vector $\mathbf{T}^{t_n}$, or $\mathbf{T}^n$ in short. Initially ($t = 0 = t_0$), $\mathbf{T}^0 = [\mathrm{NaN}, \mathrm{NaN}, \cdots, \mathrm{NaN}]^{\mathbf{T}}_{1 \times N}$, in which the subscript $\mathbf{T}$ denotes transpose and 'NaN' is short for 'not a number', indicating the element has not been deposited yet. After a period of Δt, at $t = 1 \times \Delta t = t_1$, element $P_{1,1,1}$ is deposited, the column vector is updated to $\mathbf{T}^1 = [T_n, \mathrm{NaN}, \ldots, \mathrm{NaN}]^{\mathbf{T}}_{1 \times N}$. As time increases, temperature of all elements evolves by the laws of heat transfer. FDM process finishes at t_N when all elements are deposited. When n exceeds N, with $t(n) = n\Delta t$ exceeding t_N, no more element will be deposited. For simplicity, the time required for the printing nozzle to move from the last element on one layer to the first one on the next layer is also taken as Δt.

2.2.2. Heat transfer equation

A heat transfer model is established to calculate the temperature variation in component DURING and AFTER the FDM process. With the hypotheses, settings and geometry explained above, the governing partial differential equation of transient heat transfer, derived from energy balance, is

$$\rho c_p \frac{\partial T}{\partial t} = \lambda \left(\frac{\partial^2 T}{\partial x^2} + \frac{\partial^2 T}{\partial y^2} + \frac{\partial^2 T}{\partial z^2} \right), \quad (x,y,z) \in \Omega, \tag{2}$$

in which ρ, c_p and λ denote the density, specific heat capacity (at constant pressure) and coefficient of thermal conductivity of PLA, and Ω denotes the time-dependent domain of the partial differential equation,

$$\Omega = \Omega(t) = \begin{cases} \cup P_{i,j,k}, & t \le t_N \\ 0 < x < L,\ 0 < y < W,\ 0 < z < H, & t > t_N \end{cases}. \tag{3}$$

Naturally, the boundary of the domain (Eq. (3)) ∂Ω is also time-dependent. With common finite difference method, Eq. (2) is discretized to

$$\frac{T^{n+1}_k - T^n_k}{\Delta t} = a \left(\frac{T^n_{i+1} - 2T^n_i + T^n_{i-1}}{(\Delta x)^2} + \frac{T^n_{j+1} - 2T^n_j + T^n_{j-1}}{(\Delta y)^2} + \frac{T^n_{k+1} - 2T^n_k + T^n_{k-1}}{(\Delta z)^2} \right), \tag{4}$$

in which, $a = \frac{\lambda}{\rho c_p}$, denoting the thermal diffusivity, and

$$\begin{cases} 1 \le i \le i(n),\ 1 \le j \le j(n),\ 1 \le k \le k(n), & t \le t_N \\ 1 \le i \le N_L,\ 1 \le j \le N_W,\ 1 \le k \le N_H, & t > t_N \end{cases}. \tag{5}$$

The complete form of T^n_{i+1} in Eq. (4) is $T^n_{i+1,j,k}$, etc. The essence of Eq. (4) states that the temperature of element $P_{i,j,k}$ at t_{n+1} is determined by a linear combination of the temperature of itself and its six neighbors at t_n. A neighbor element of $P_{i,j,k}$ is one who shares a common face with $P_{i,j,k}$. For an interior element $P_{i,j,k}$, all its neighbor elements are $P_{i\pm1,j,k}$, $P_{i,j\pm1,k}$, and $P_{i,j,k\pm1}$. For the sake of discussion in the following sections, element $P_{i,j,k+1}$ is identified as primary neighbor. For boundary elements, their neighbors could either be air or heat plate. Denoting the ± x, ± y and ± z directions as 'front and back', 'left and right', 'up and down', respectively, then Eq. (4) could be rearranged for direct iteration as

$$T^{n+1}_{i,j,k} = f_x \times (T^n_{\text{front}} + T^n_{\text{back}}) + f_y \times (T^n_{\text{left}} + T^n_{\text{right}}) + f_z \times (T^n_{\text{up}} + T^n_{\text{down}}) + [1 - 2(f_x + f_y + f_z)]T^n_{i,j,k} \tag{4$_*$}$$

Table 1
Temperature calculation procedure, taking $N_L = 3, N_W = 2$ and $N_H = 3$ as example.

ID n	Position			Neighbor position						t_0		t_1		t_2		…
	i	j	k	Up	Down	Front	Back	Left	Right	T^{t_0}	Age^0	T^{t_1}	Age^1	T^{t_2}	Age^2	
1	1	1	1	1,1,2	1,1,0	2,1,1	0,1,1	1,2,1	1,0,1	NaN	0	T_n	1	?	2	…
2	2	1	1	2,1,2	2,1,0	3,1,1	1,1,1	2,2,1	2,0,1	NaN	−1	NaN	0	T_n	1	…
3	3	1	1	3,1,2	3,1,0	4,1,1	2,1,1	3,2,1	3,0,1	NaN	−2	NaN	−1	NaN	0	…
4	3	2	1	3,2,2	3,2,0	4,2,1	2,2,1	3,3,1	3,1,1	NaN	−3	NaN	−2	NaN	−1	…
5	2	2	1	2,2,2	2,2,0	3,2,1	1,2,1	2,3,1	2,1,1	NaN	−4	NaN	−3	NaN	−2	…
6	1	2	1	1,2,2	1,2,0	2,2,1	0,2,1	1,3,1	1,1,1	NaN	−5	NaN	−4	NaN	−3	…
7	1	1	2	1,1,3	1,2,1	2,1,2	0,1,2	1,2,2	1,0,2	NaN	−6	NaN	−5	NaN	−4	…
…	…			…						…	…	…	…	…	…	…
N	$1/N_L$	N_W	N_H	…						NaN	$N+1$	NaN	$N+2$	NaN	$N+3$	…

in which, $f_x = \frac{a\Delta t}{(\Delta x)^2}$, $f_y = \frac{a\Delta t}{(\Delta y)^2}$, $f_z = \frac{a\Delta t}{(\Delta z)^2}$.

In Eq. (2), the density ρ and specific heat capacity c_p of PLA change drastically when temperature drops from above melting temperature to below the temperature of glass transition. Given experimental measurement and mathematical technique of spline interpolation, the dependence of these properties on temperature are considered known and will be updated according to local temperature in calculation (Fig. S1, supporting information). Thermal conductivity of PLA is taken constant to be $\lambda = 1.95 \times 10^{-4} \frac{\mathrm{W}}{\mathrm{m\,K}}$ [25] when PLA solidified from polymer melt to glass state.

2.2.3. Initial and boundary condition

For a single element, the initial temperature upon deposition is assumed uniform and equal to the nozzle temperature, T_n. The union of all deposited elements make up the FDM component.

Type 1 boundary condition is chosen for the complex moving boundary during FDM. A boundary-adjusting technique is employed, as when the geometry domain $\Omega = \Omega(t)$ is developing during FDM in an additive manner, the boundary of such domain also updates as time evolves, $\partial\Omega = \partial\Omega(t)$. In essence, the temperature of elements surface is taken to be T_p if it is in contact with the heat plate, and T_a if in in contact with air,

$$T(\partial\Omega) = \begin{cases} T_p, & \text{contacting heat plate} \\ T_a, & \text{contacting the air} \end{cases}.$$

2.3. Algorithm and stability

2.3.1. Algorithm of the solution

Two stages of algorithm are required in calculation, because during and after FDM, the geometry domains are different by Eq. (3). An interior element when FDM is done could be a boundary element during FDM or even not-yet deposited.

The temperature calculation procedure is illustrated in Table 1, in which, each element is assigned with five properties: the ID (n), position (i,j,k), neighbor position, temperature T and age. The last

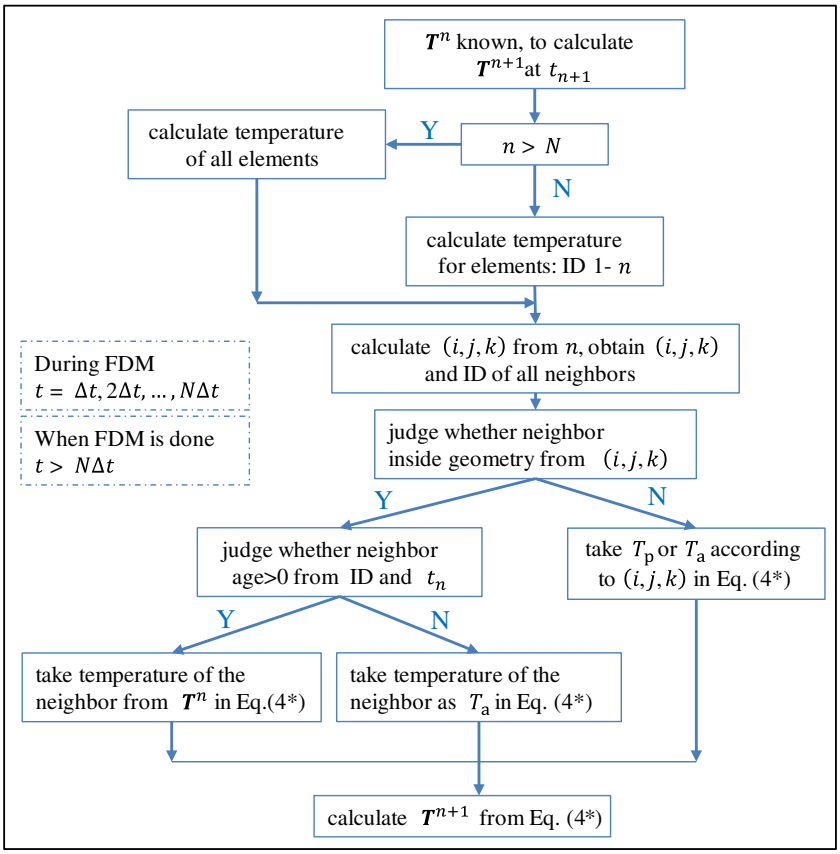

Fig. 2. Flow chart of the key idea of the algorithm to calculate T^{n+1} from T^n.

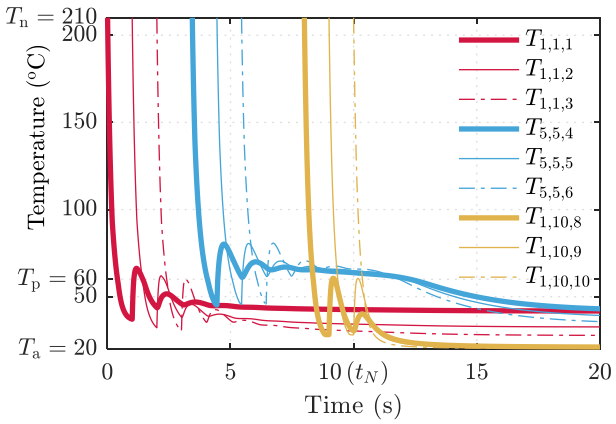

Fig. 3. Reheating of elements by their neighbor elements above.

two are dynamic properties, while the others are static. The property 'age' is introduced to judge whether as element have been deposited. For an element at any moment, age > 0 indicates this element has been deposited, age ≤ 0 indicates otherwise. At $t = 0 = t_0$, the age of all elements is initially set 0, -1, -2, …, $-N+1$. When time increases by Δt, the age of all elements increase by 1. When the age of the element P_N becomes 1, the FDM process is complete.

Fig. 2 summarizing key ideas of the algorithm to calculate $\boldsymbol{T}^{n+1}$ from $\boldsymbol{T}^n$ is attached for better understanding.

2.3.2. Stability of the algorithm

The stability of the scheme of Eq. (4$_*$) is discussed for $t \geq t_N$, when FDM is complete and the component geometry is fixed.

The scheme of the finite difference method behind Eq. (4$_*$) could be written in the form of matrix multiplication

$$\boldsymbol{T}^{n+1} = \boldsymbol{A}\boldsymbol{T}^n + \boldsymbol{F}, \tag{6}$$

in which, $n \geq N$, and $\boldsymbol{T}^n$ denotes the temperature of all elements at time t_n. $\boldsymbol{F}$ is a constant column vector of the same dimension as $\boldsymbol{T}^n$ ($N \times 1$), given the constant thermal boundaries. Most entries of vector $\boldsymbol{F}$ are 0, while the none-zero entries correspond to the calculation of the temperature of boundary elements. $\boldsymbol{A}$ is a real symmetric constant tri-diagonal block matrix, the dimension of which is $N \times N$,

$$\boldsymbol{A} = \begin{bmatrix} \boldsymbol{M} & \boldsymbol{R} & & & \\ \boldsymbol{R} & \boldsymbol{M} & \boldsymbol{R} & \ddots & \\ & \ddots & \ddots & & \\ & & \boldsymbol{R} & \boldsymbol{M} & \boldsymbol{R} \\ & & & \boldsymbol{R} & \boldsymbol{M} \end{bmatrix}_{N\times N}, \text{ in which } \boldsymbol{M} = \begin{bmatrix} \boldsymbol{Q} & \boldsymbol{P} & & & \\ \boldsymbol{P} & \boldsymbol{Q} & \boldsymbol{P} & \ddots & \\ & \ddots & \ddots & & \\ & & \boldsymbol{P} & \boldsymbol{Q} & \boldsymbol{P} \\ & & & \boldsymbol{P} & \boldsymbol{Q} \end{bmatrix} \text{ and}$$

$$\boldsymbol{R} = \begin{bmatrix} f_z & & & & \\ & f_z & & & \\ & & \ddots & & \\ & & & f_z & \\ & & & & f_z \end{bmatrix}.$$

Matrices $\boldsymbol{M}$ and $\boldsymbol{R}$ have the same dimension of $N_L N_W \times N_L N_W$. $\boldsymbol{M}$ is also a real symmetric constant tri-diagonal block matrix. The block entries $\boldsymbol{P}$ and $\boldsymbol{Q}$ are smaller matrices of the dimension $N_L \times N_L$. $\boldsymbol{Q}$ is another tri-diagonal matrix with constant entries, while $\boldsymbol{P}$ is a diagonal matrix. Denoting $q \equiv 1 - 2(f_x + f_y + f_z)$ in Eq. (4$_*$), then,

$$\boldsymbol{Q} = \begin{bmatrix} q & f_x & & & \\ f_x & q & f_x & \ddots & \\ & \ddots & \ddots & & \\ & & f_x & q & f_x \\ & & & f_x & q \end{bmatrix}_{N_L\times N_L} \text{ and } \boldsymbol{P} = \begin{bmatrix} f_y & & & & \\ & f_y & & & \\ & & \ddots & & \\ & & & f_y & \\ & & & & f_y \end{bmatrix}_{N_L\times N_L}.$$

For the discussion of stability, Eq. (6) is rewritten into Eq. (6$_*$) by considering adding a layer of paddings of air or heat plate glass elements of constant temperature of T_a or T_p to the component,

$$\widetilde{\boldsymbol{T}}^{n+1} = \widetilde{\boldsymbol{A}}\,(\widetilde{\boldsymbol{T}}^n), \tag{6$_*$}$$

in which, $\widetilde{\boldsymbol{T}}^n$ denotes the temperature of all elements (including air and glass element) at time t_n. The dimension of matrix $\widetilde{\boldsymbol{A}}$ is $[(N_L+2)(N_W+2)(N_H+2)]^2$. $\widetilde{\boldsymbol{A}}$ differs from matrix $\boldsymbol{A}$ slightly in rows, as basically, $\widetilde{\boldsymbol{A}}$ consists of row vectors in the form of $[\cdots, f_z, \cdots, f_y, \cdots, f_x, q, f_x, \cdots, f_y, \cdots, f_z, \cdots]$ and $\boldsymbol{e}^{\mathbf{T}}$, the basic row vector of identity matrix $\boldsymbol{I}$ of the same dimension as $\widetilde{\boldsymbol{A}}$. $\widetilde{\boldsymbol{A}}$ is also a real symmetric matrix as $\boldsymbol{A}$ is, its eigenvalues are all real. Eq. (6$_*$) essentially combines the influence of vector $\boldsymbol{F}$ on matrix multiplication in Eq. (6) into the matrix, and could be iterated as.

$$\widetilde{\boldsymbol{T}}^n = (\widetilde{\boldsymbol{A}})^{n-N}\widetilde{\boldsymbol{T}}^N. \tag{6$_{**}$}$$

Stability of the algorithm requires the matrix $(\widetilde{\boldsymbol{A}})^{n-N}$ in Eq. (6$_{**}$) is bounded as $n \to \infty$. (The superscript over a vector denotes the time, while the superscript over the matrix denotes multiplication.) If $q \equiv 1 - 2(f_x + f_y + f_z) \geq 0$, then by Gerschgorin theorem, all real eigenvalues λ_j of matrix $\widetilde{\boldsymbol{A}}$ satisfy $|\lambda_j| - q \leq |\lambda_j - q| \leq 2(f_x + f_y + f_z)$ or $|\lambda_j - 1| \leq 0$, which means $|\lambda_j| \leq 1$ for $j = 1, 2, \cdots, [(N_L+2)(N_W+2)(N_H+2)]^2$, and thus $(\widetilde{\boldsymbol{A}})^{n-N}$ is bounded as the calculation proceeds. However, if $q < 0$, $|\lambda_j| \leq 1$ for all j cannot be guaranteed, and the matrix multiplication will blow up sometime. As a brief conclusion, the stability of the algorithm requires.

$$a\Delta t\left[\frac{1}{(\Delta x)^2} + \frac{1}{(\Delta y)^2} + \frac{1}{(\Delta z)^2}\right] \leq 0.5. \tag{7}$$

3. Results and discussion

Taking $\Delta x = 0.4$ mm in the mathematical model, with the algorithm explained above, temperature variation of the FDM constructed component during and after FDM is calculated and shown below. The stability requirement by inequality (7) is met for all simulated components subjected to different parametric settings.

3.1. Reheating effect

As FDM process constructs components in an additive manner, the phenomenon of reheating of a cooler raster by a lately deposited hotter one is universal. To give an example, taking elements $P_{1,1,1}$, $P_{5,5,4}$ and $P_{1,10,8}$ in interested rasters, their temperature profiles are displayed in Fig. 3 along with the temperature profiles of their primary neighbor elements (elements located vertically above).

As reported from [18,20], the local temperature of FDM component was monitored/analyzed to undergo considerable wave-like variation, and was explained by the reheating effect of a newly deposited element on heat transfer. In the simulation shown in Fig. 3, the temperature of element $P_{5,5,4}$ decreases rapidly since its deposition. After a period of time of t_N/N_H, when the primary neighbor element above $P_{5,5,5}$ is deposited, heat flows from the newborn element to the cooler one since there exists considerable temperature difference. When the primary neighbor of $P_{5,5,5}$, i.e. $P_{5,5,6}$, is deposited, the same reheating effect happens to $P_{5,5,6}$ and is transferred downwards, raising the temperature of element $P_{5,5,4}$ again. This kind of reheating phenomenon is identified as primary reheating effect. Primary reheating is universal (for both inner element $P_{5,5,4}$, and boundary elements $P_{1,1,1}$ and $P_{1,10,8}$) in FDM. Whenever an element is deposited, the elements below will be reheated. The longer the distance, the weaker the influence. Penetration depth of primary reheating effect is approximately three layers in the deposition of the geometry with default settings.

When FDM is done, the temperature field inside the component gradually approaches some steady state, where the temperature of element $P_{5,5,4}$, $P_{5,5,5}$ and $P_{5,5,6}$ is predicted to be in a descending order since their distance to the heat plate ascends ($T_a < T_p$).

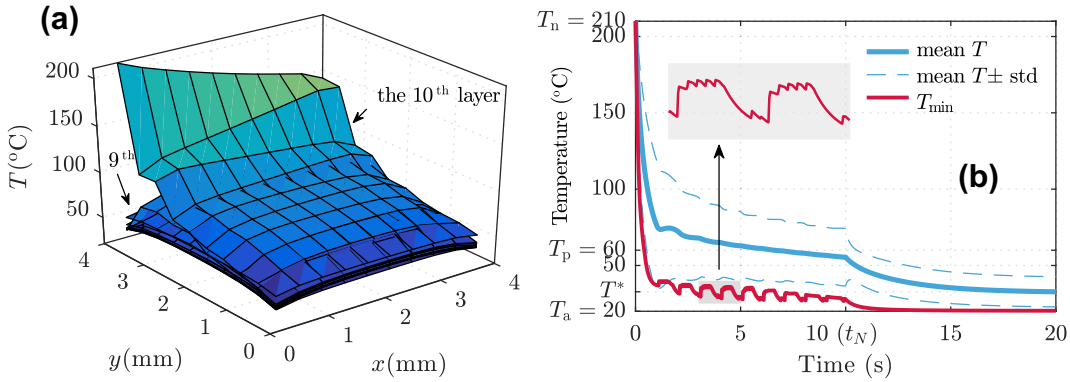

Fig. 4. (a) Temperature field at $t = t_N$, displayed layer by layer; (b) mean temperature and other characteristics of the component from $t = 0$ to $t = 2t_N$.

3.2. $T = T(\boldsymbol{x}, t)$, cooling rate and ∇T

Temperature variation with respect to space and time $T(\boldsymbol{x}, t)$ is approximated by $T_i^{t_n}, j, k$ calculated from the algorithm aforementioned. Upon finishing $T(\boldsymbol{x}, t_N)$ is presented by T_i^N, j, k, displayed layer by layer in Fig. 4(a); variation of mean temperature $\overline{T}(t)$ of the printed component from $t = 0$ to $t = 2t_N$ is displayed in Fig. 4(b). The mean temperature at time t_n of the component is defined and approximated by the volume-averaged temperature of all deposited elements,

$$\overline{T}(t) \equiv \frac{1}{V}\iiint_{\Omega} T(\boldsymbol{x}, t_n)\mathrm{d}x\mathrm{d}y\mathrm{d}z \approx \frac{1}{n}\sum_{i,j,k} T_{i,j,k}^{t_n},$$

in which, Ω is the geometry of the deposited component defined in Eq. (3), V is the volume of such geometry, n is the number of elements deposited by t_n, and (i,j,k) are functions of time t_n defined in Eq. (5).

Due to relatively small dimension (dimensional effect is discussed later), the temperature of all elements decreases rapidly towards the boundary (heat plate and the air) temperature. Temperature difference between the latest deposited two layers is huge (Fig. 4(a)). When a new layer is deposited, the previous layer has cooled extensively. Upon contact, heat is transferred through conduction, while at the same time dissipates into the environment. The overall energy of the polymer in the interface may be insufficient for molecule chain to make enough fusion and coalescence, resulting in inferior interface. This assumed situation could explain the common phenomenon of poor inter-layer bonding reported in many literatures [26,27], which compromises macro physical-mechanical properties. Fig. 4(a) also reveals that the temperature of elements in the interior region of the component is usually higher than that near the boundary, as $T_a < T_p$ is default.

The overall temperature of the component is depicted as the mean temperature, shown in Fig. 4(b), decrease of which in FDM is rapid and comparable to exponential decay. The mean temperature experiences small scale wave-like fluctuation, resulting from the reheating effect. The minimum temperature among all elements exhibits a similar decreasing pattern, however, shows two orders of fluctuation, as reported in the experimental investigation in [12]. The primary fluctuation results from primary reheating effect between up and down layers, while the secondary one results from secondary reheating by the neighbors of primary neighbor. Soon after FDM is complete, the minimum temperature approaches the environment temperature T_a very rapidly (see also Fig. S2), while the mean temperature decreases steadily and smoothly towards T^* (somewhere between T_a and T_p, Figs. 4(b) and 5(a)). Given constant boundary conditions, standard deviation of the mean temperature also tends to stabilize when the time approaches $2t_N$, showing the steady state is approached.

3.2.1. Cooling rate

Overall cooling rate β of component by FDM is a derived parameter from temperature variation, defined as the derivative of mean temperature of deposited component with respect to time, $\beta(t) = \frac{\mathrm{d}\overline{T}(t)}{\mathrm{d}t}$. A 'central difference' finite difference method and a 'fitting & differentiate' method are employed to estimate the overall cooling rate (Fig. S3).

Assuming a one-to-one mapping between the mean temperature $\overline{T}(t)$ and the time t (Not strictly true), $\beta(t) = \beta(t(\overline{T})) = \beta(\overline{T})$, and thus, the variation of overall cooling rate with respect to mean temperature is shown in Fig. 5(a), in which, cooling rate β decreases with decrease of the difference between the mean temperature and boundary temperature. The cooling rate at earlier stage when depositing the 1st layer is estimated to be of the order of 10^2°C/s. When the mean temperature drops to near the heat plate temperature T_p, β decreases by two orders of magnitude, down to 10^0°C/s. Upon finishing, $\beta \approx 30$°C/min by the 'central difference' method, which could be a lower limit, and $\beta \approx 100$°C/min by the 'fitting & differentiate' method, which could be considered a characteristic cooling rate of FDM, given the default settings in the model.

The influence of cooling rate on inter-layer bonding strength and crystallization of the polymer is profound, but stills need more elaborations. To give an example, we have detected a threshold of cooling rate of 10°C/min for semi-crystalline polymer PLA (3052D, NatureWorks) in experiments, above which crystallization will not happen during cooling from polymer melt (thus hypothesis 1 makes perfect sense, see also Fig. S4). Crystallization of semi-crystalline thermoplastic polymer is a crucial aspect in FDM as it can affect both energy balance and thermal deformation significantly.

3.2.2. Temperature gradient

Temperature gradient $\nabla T = [T_x, T_y, T_z]$ is approximated with a combination of first and second order finite difference discretization. For example, at the center of element $P_{i,j,k}$ at time t_n, $T_x(i,j,k) \approx \frac{T_{i+1,j,k}^n - T_{i-1,j,k}^n}{2\Delta x}$ for interior elements, and $T_x(i,j,k) \approx \frac{T_{i+1,j,k}^n - T_{i,j,k}^n}{\Delta x}$ or $T_x(i,j,k) \approx \frac{T_{i,j,k}^n - T_{i-1,j,k}^n}{\Delta x}$ for boundary elements. Temperature gradient is presented as the intensity of it with respect to space, i.e., $|\nabla T| = (T_x^2 + T_y^2 + T_z^2)^{\frac{1}{2}}$, shown in Fig. 5(b–d).

Upon finishing, on layer 1–7, temperature gradient intensity $|\nabla T|$ is of the order of 10°C/mm for elements away from the boundary, and 30°C/mm for elements near/on the boundary. On the last three layers, the temperature gradient intensity everywhere is higher by 1–2 orders, up to 1000°C/mm (Fig. 5(b)). However, temperature gradient intensity in the newly deposited component will soon die away due to rapid cooling. At characteristic moment of $2t_N$, it is generally high on lower layers but low on higher layers (Fig. 5(d)), of the order of 5–50°C/mm.

Readers can also consult GIF pictures included in the supporting information for direct observation of the temperature field and temperature gradient intensity variation with respect to space at other characteristic moments in FDM.

Temperature gradient is thought to be responsible for the common wrapping, distortion phenomena of the components in FDM [15,16], through the mechanics of thermo-elasticity. We will pay more attention on this aspect.

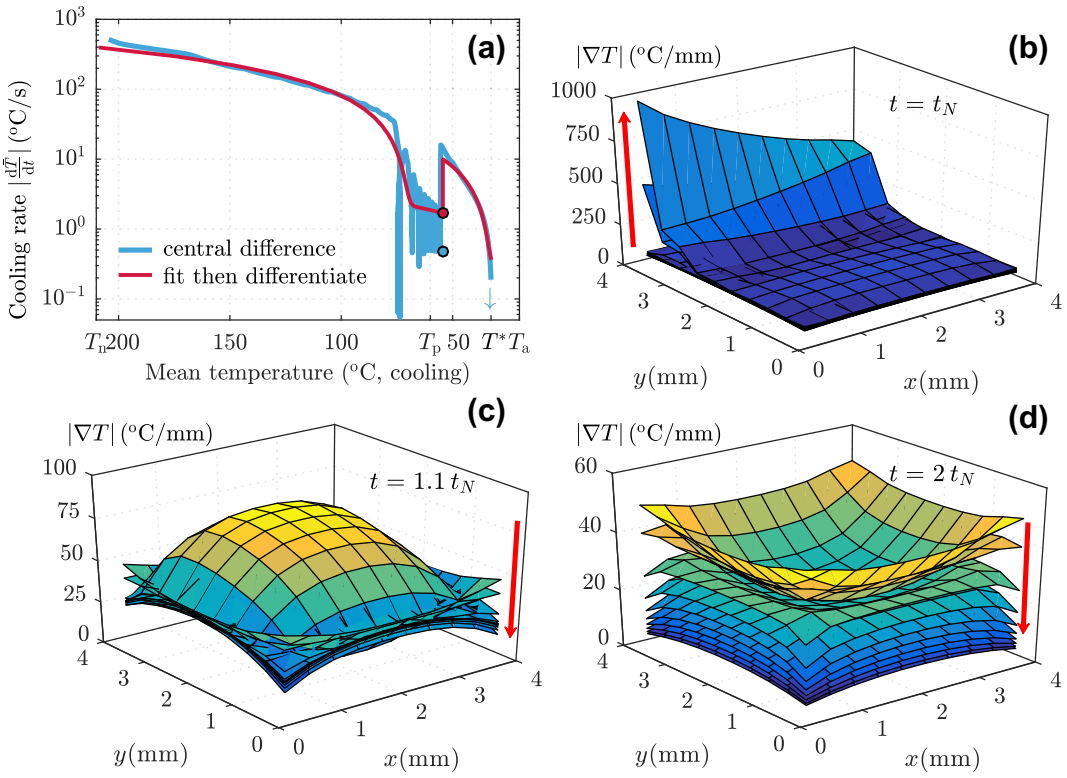

Fig. 5. Overall cooling rate of the component (a) and temperature gradient intensity at various characteristic moments (b–d). The directions shown by red arrows in the figure indicate the layer number in an ascending order, from the 1st layer to the 10th. (For interpretation of the references to color in this figure legend, the reader is referred to the web version of this article.)

3.3. Influence of temperature of printing nozzle, heat plate and environment

Temperature settings are primary factors determining the temperature variation.

Nozzle temperature T_n defines initial temperature when FDM begins. T_n should be higher than the melting temperature T_m of the polymer, so as to enable the thermoplastic to flow out of the printing nozzle under pressure, while at the same time, lower than the onset temperature of thermal decomposition T_{onset}, in order to avoid major thermal decomposition. A least restrictive criterion for setting the nozzle temperature is $T_m < T_n < T_{onset}$. To ensure FDM applicable, $T_a, T_p < T_n$ is usually required, so that polymer melt could solidify with the decrease of internal energy. By solely changing T_a or T_p to different values in the default settings, this mathematical model would give different temperature variation patterns, assuming no rheological setbacks. For comparison, these mean temperature profiles are presented in Fig. 6.

When changing the thermal boundary, either the environment or heat plate temperature, the mean temperature exhibits different patterns, in which, the overall cooling rate differs case by case, and the temperature gradient may also exhibit unique characteristics in different settings. Two extreme cases tell that when boundary temperature is relatively high ($T_a = 100\,^{\circ}C$ and $T_p = 60\,^{\circ}C$, Fig. 6(a)), overall cooling rate is relatively low and temperature gradient may be less steep throughout; when boundary temperature is relatively low ($T_a = T_p = 20\,^{\circ}C$, Fig. 6(b)), cooling of the component is more intense.

These simulated changes of the boundary temperature settings are enlightening for practical applications of FDM, as the case of $T_a = 100\,^{\circ}C$, $T_p = 60\,^{\circ}C$ would depict the thermal process of FDM performed in boiling water, as long as there is no undesired implication

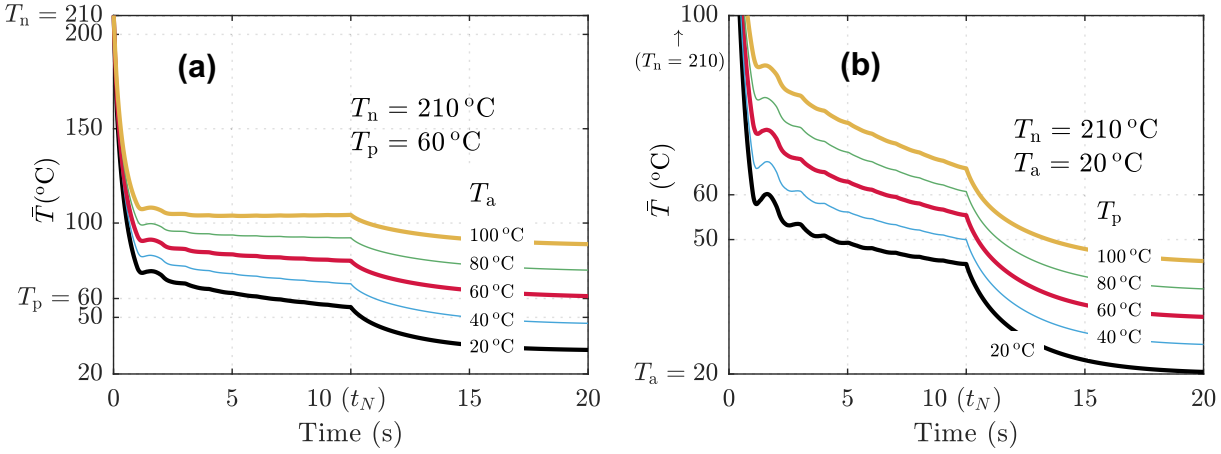

Fig. 6. Variation of mean temperature of the component with respect to time when FDM progresses at different environment temperature (a) and heat plate temperature (b).

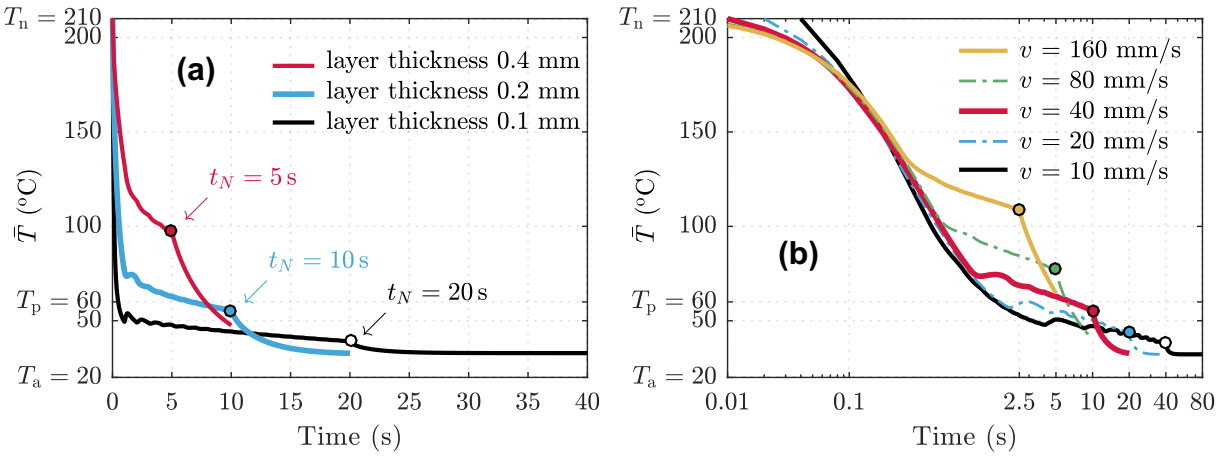

Fig. 7. Influence of layer thickness (a) and printing speed (b) on mean temperature variation.

in the new environment. But most basically, in order to ensure the temperature variation to match a prescribed pattern for whatever the purpose (e.g. controlled degree of coalescence or crystallinity), T_a and T_p could be fine-tuned to complete the mission.

3.4. Influence of layer thickness and printing speed

Layer thickness and printing speed are two parameters that constantly adjusted in FDM. They can also affect the FDM process significantly. By only changing layer thickness or printing speed to different values in the default settings, the mean temperature variation simulated with the model is presented in Fig. 7.

Layer thickness and printing speed affect the (mean) temperature variation in FDM in a similar way, the higher the layer thickness or printing speed, the lower the time required to finish FDM and the higher the mean temperature of the component upon finishing. Higher mean temperature of the component is beneficial for inter-layer coalescence, as a result, higher layer thickness usually correlates to higher mechanical performance [1]. Inter-layer cooling time is reported to be negatively correlated with mechanical properties of FDM constructed components [28]. The high the printing speed, the lower the inter-layer cooling time. Although the influence of printing speed is rarely studies, this result would predict printing speed to be positively correlated to (at least) mechanical properties of FDM constructed components, assuming no rheological problems.

Layer thickness and printing speed to some extent can compensate with each other, allowing more freedom in controlling temperature variation of the component in FDM.

3.5. Influence of dimensional effect

The influence of dimensional effect on the thermal process in FDM is twofold.

For the first aspect, the temperature variation of the macro component to-be-deposited is self-affected by its own geometry dimension.

To elaborate, we include the mean temperature profile of the common specimen required in the standard test of plastic flexural property, of the dimension $80 \times 10 \times 4$(mm), in Fig. 8(a), labeled as 'Geometry 2', as a contrast to the mean temperature profile of geometry with the default settings, labeled as 'Geometry 1'. For Geometry 2, due to (relatively) larger cross section area, the building time of each layer is 50(s), much longer than that required in Geometry 1. Longer inter-layer building time allows the freshly deposited layer to cool extensively. When a new layer is deposited, the reheating effect will be more significant, even on a macro-geometry level. In the shading area in Fig. 8(a), there are exactly 19 times abrupt increase of mean temperature during the additive deposition of 20 layers in total. The penetration depth of the primary reheating effect in Geometry 2 is unlimited compared with the case in Geometry 1 (Fig. 3). Temperature profile of an exemplary element $P_{6,13,10}$ in Geometry 2 is displayed in Fig. 8(b), in which, primary reheating effect resulting from deposition of primary neighbors (neighbors located above, i.e. $P_{6,13,11}$, $P_{6,13,12}$, …, $P_{6,13,20}$) is profound, but the influence decays exponentially with the vertical distance. The secondary reheating effect, shown in the subplot in Fig. 8(b), is caused by the deposition of the neighbor of primary neighbors in the direction perpendicular to the nozzle movement on the same layers (Fig. 8(c)). The secondary reheating effect is scaled by spatial distance somehow sinusoidally. From the intensity of reheating effect in different directions, one can concur the intensity of heat conduction ascends in x, y and z directions in such a geometry given the settings. Besides, secondary reheating effect also reminds that when measuring local temperature profile in FDM, the frequency of such measurement system should be high enough and in proportion to printing speed.

To exemplify the influence of prolonged inter-layer cooling time, there are researches [27,28] stating the problems encountered when depositing components with wide cross sections of dimension up to 10^0m × 10^0m. In those situations, rapid cooling of a deposited layer due to long period of building of bigger cross section led to poor inter-layer bonding and ultimately compromised mechanical strength in z direction. Solutions like infrared preheating [27] or layer-assisted heating [29] were proposed and found effective, but in essence, careful control of FDM parameters like printing speed and especially heat plate temperature and the environment temperature can avoid such problem from the very beginning.

The second aspect of the dimensional effect pertains to the influence of the resolution of a FDM printer on the temperature variation. The resolution of FDM printer could be taken as the finest structure possibly deposited by a FDM printer. With default settings in the model–printing nozzle diameter of 400 μm, layer thickness of 200 μm–the resolution of such FDM printer can be taken of the magnitude of 10^2μm. Higher resolution inversely corresponds to smaller space dimension.

Cutting-edge applications of FDM may require higher order of resolution, but the limit to the resolution of a FDM printer is not completely known to date. From the perspective of energy balance and bond formation, a limiting factor could be temperature management. Assuming FDM printers of higher and lower resolution are invented somehow (higher resolution: printing nozzle diameter 40 μm, resolution 10 μm; lower resolution: printing nozzle diameter 4000 μm, resolution 1000 μm), and used together with current commercial FDM printer. The mean temperature profiles of the components constructed by these FDM printers differ significantly, shown in Fig. 8(d). In the simulations, the geometry of the component and basic element is scaled by resolution while all the other settings remain the same.

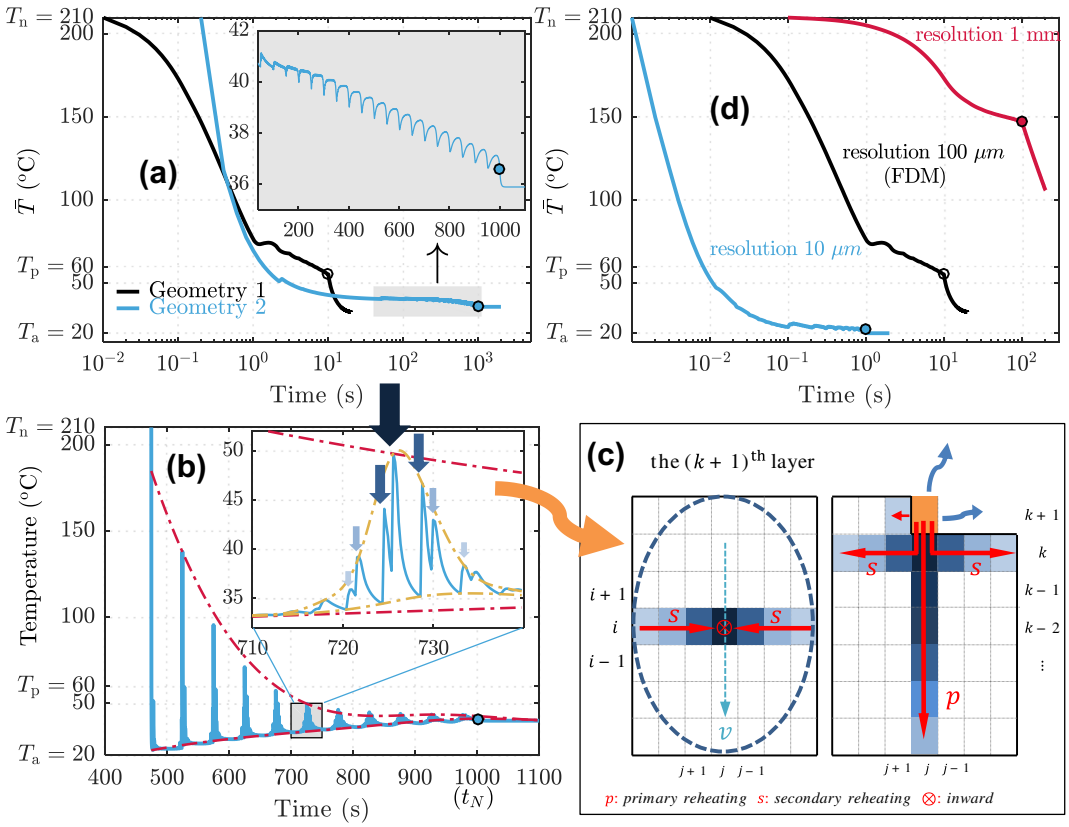

Fig. 8. Influence of geometry dimension on temperature development. (a) Mean temperature variation for different geometries. 'Geometry 1' is of dimension 4 × 4 × 2(mm), 'Geometry 2' 80 × 10 × 4(mm); (b) temperature profile of element $P_{6,13,20}$ in Geometry 2; (c) a diagram to explain secondary reheating effect; (d) temperature variation in FDM at different resolutions.

When the resolution of a FDM printer is low, such FDM process may fall into the concept of traditional plastic processing technique. The temperature decrease is much slower, as depicted in Fig. 8(d), the consequence of polymer crystallization and subsequent thermo-mechanical phenomena should be taken care of.

When the resolution is high, the dimension of the geometry is small, heat conduction within the component is rapid. Similar to the illustrative case of unsteady, spherically symmetric heat flow in [30], the cooling rate is inverse proportional to the square of the resolution, $\beta \propto \text{resolution}^{-2}$, given constant boundary conditions. This implies temperature management will be much more demanding in the case of higher resolution. If simply replace the printing nozzle of diameter 40 μm, and proceed FDM without modifying the temperature of the environment and heat plate, the extruded rasters of polymer melt will solidify instantly (Fig. 8(d)) due to super fast heat conduction, and the deposited component will presumably have no internal bonding at all, probably appear in the form of stacked hairs. As inspired from previous analyses, strict temperature management through careful control of $T_a = T_a(\boldsymbol{x}, t)$ and $T_p = T_p(\boldsymbol{x}, t)$ in FDM process is necessary in the application of FDM printer of higher resolution.

3.6. Improvement of the model: go multi-scale

In this model, only the dimension of the sub-milli-metrical element in x direction could vary freely. This would naturally cause doubts on the convergence of the finite difference scheme. A multi-scaled modeling method could be adopted to eliminate this doubt.

Referring to Fig. 1(b), the sub-milli-metrical element is segmented into smaller micro elements of dimension $\delta x = \frac{\Delta x}{m_1}$, $\delta y = \frac{\Delta y}{m_2}$, and $\delta z = \frac{\Delta z}{m_3}$. m_1, m_2 and m_3 are positive integers denoting the number of micro element in x, y and z direction in the sub-milli-metrical element. The smaller micro element is the fundamental unit of the multi-scaled model, and will be assumed to have uniform temperature distribution at any moment. By such a multi-scale method, the model differs from the previous one only in the boundary condition of the basic unit, as the micro elements on the same $y - z$ plane within the same extruded raster are deposited simultaneously but have different thermal boundaries. The governing equation and initial condition remains the same. Such a multi-scaled model can guarantee the numerical solution converge to the real one as the number of micro element in each direction goes to infinity. Temperature distribution within a single raster in FDM could also be studied, which may provide more insight in the coalescence between adjacent layers. In the multi-scale model, m_1 could simply take the value of 1. However, limited by the hypothesis of continuum mechanics, the value of m_2 and m_3 should not be too big, recommend magnitude is of 10^1. If exceeded this scale even by one magnitude, apart from possible risk of breaking physical conception of continuum, the calculation time and storage of the results would be much demanding.

Other improvement from the perspectives of raster angle, filling ratio, boundary condition and exclusion of hypothesis 1 are provided in the supporting discussion.

4. Conclusions

This paper presents an adaptable three-dimensional transient mathematical model of temperature development during and after the fused deposition modeling with a boundary-adjusting finite difference method. With such a model, researchers can better understand the thermal process of FDM from the perspective of energy balance, through the study of almost every influential parameter currently available. Some predicted but significant qualitative conclusions are drawn, many of which have never been revealed from previous experiments or analysis.

- Reheating effect of a deposited raster by a newly deposited one is universal phenomenon, and happens mainly in the layer thickness direction. The higher the temperature difference between adjacent

layers, arising from either temperature settings, big cross-section area, low printing speed or thin layer thickness, the more obvious the reheating effect. To measure secondary reheating effect, the frequency of such measurement system should be high enough, and in proportion to printing speed.

- Temperature settings (temperature of printing nozzle, temperature of heat plate and the environment) are crucial factors determining temperature variation. Careful control of temperature of heat plate and the environment can help to reduce the temperature gradient as well as to control the overall cooling rate, for the further purpose of reducing internal stress inside the component or promoting inter-layer bonding strength, and ultimately improving the feasibility of FDM application.
- In FDM, the higher the layer thickness or printing speed, the lower the overall cooling rate. These two parameters could be adjusted complementarily or simultaneously in practice, to allow more freedom in temperature control. Printing speed is also predicted to be positively correlated to mechanical properties of FDM constructed components through the mechanism of thermal coalescence.
- If a FDM printer of higher resolution is to be invented and applied, the temperature control system should be well-controlled to prevent rapid heat dissipation due to dimensional effect during the FDM process.

Such a numerical investigation of the influence of process conditions on the temperature variation with respect to space and time in FDM can provide immediate guidance over current applications of FDM. Significant physical phenomena such as bond formation and mechanical deformation could also be studied from the perspective of energy balance on the basis of this numerical model, especially when direct temperature measurement is challenging. More profoundly, understand temperature variation is beneficial and fundamental to the full understanding of the mechanics of FDM.

Acknowledgements

This research is financially supported by Zhejiang Key Level 1 Discipline of Forestry Engineering (2014lygcy022). The authors would like to thank retired professor Yu, Changming from School of Energy and Environment Engineering, University of Science and Technology Beijing, for helpful and inspiring discussion on the heat transfer model in fused deposition modeling. Special thanks go to Miss Huang, Jue from the College of Art & Design, Nanjing Forestry University, for her dedicated help in diagram design. Comments and suggestions from reviewers are also acknowledged.

Appendix A. Supplementary data

Supplementary data to this article can be found online at http://dx.doi.org/10.1016/j.matdes.2017.05.040.

References

[1] O. Carneiro, A. Silva, R. Gomes, Fused deposition modeling with polypropylene, Mater. Des. 83 (2015) 768–776 http://dx.doi.org/10.1016/j.matdes.2015.06.053.
[2] L. Novakova-Marcincinova, I. Kuric, Basic and advanced materials for fused deposition modeling rapid prototyping technology, Manuf. Ind. Eng. 11 (1) (2012) 25–27.
[3] W.W. Yu, J. Zhang, J.R. Wu, Y.H. Deng, Incorporation of graphitic nano-filler and poly(lactic acid) in fused deposition modeling, J. Appl. Polym. Sci. 134 (15) (2017), http://dx.doi.org/10.1002/app.44703.
[4] A.L. Duigou, M. Castro, R. Bevan, N. Martin, 3D printing of wood fibre biocomposites: from mechanical to actuation functionality, Mater. Des. 96 (2016) 106–114, http://dx.doi.org/10.1016/j.matdes.2016.02.018.
[5] P.C. Hsieh, C.H. Tsai, B.H. Liu, W.C.J. Wei, A.B. Wang, R.C. Luo, 3D Printing of low Melting Temperature Alloys by Fused Deposition Modeling, 2016 IEEE International Conference on Industrial Technology (ICIT), Taipei, (2016), http://dx.doi.org/10.1109/ICIT.2016.7474915.
[6] A.S. Bala, S.B. Wahab, M.B. Ahmad, Elements and materials improve the FDM products: a review, Adv. Eng. Forum. 16 (2016) 33, http://dx.doi.org/10.4028/www.scientific.net/AEF.16.33.
[7] R.K. Sahu, S. Mahapatra, A.K. Sood, A study on dimensional accuracy of fused deposition modeling (FDM) processed parts using fuzzy logic, Int. J. Manuf. Sci. Prod. 13 (3) (2013) 183–197, http://dx.doi.org/10.1515/jmsp-2013-0010.
[8] O.A. Mohamed, S.H. Masood, J.L. Bhowmik, Optimization of fused deposition modeling process parameters for dimensional accuracy using I-optimality criterion, Measurement 81 (2016) 174–196 http://dx.doi.org/10.1016/j.measurement.2015.12.011.
[9] A.K. Sood, R.K. Ohdar, S.S. Mahapatra, Parametric appraisal of mechanical property of fused deposition modelling processed parts, Mater. Des. 31 (1) (2010) 287–295, http://dx.doi.org/10.1016/j.matdes.2009.06.016.
[10] B.N. Panda, K. Shankhwar, A. Garg, J. Zhang, Performance evaluation of warping characteristic of fused deposition modelling process, Int. J. Adv. Manuf. Technol. 88 (2017) 1799–1811, http://dx.doi.org/10.1007/s00170-016-8914-8.
[11] Q. Sun, G.M. Rizvi, C.T. Bellehumeur, P. Gu, Effect of processing conditions on the bonding quality of FDM polymer filaments, Rapid Prototyp. J. 14 (2) (2008) 72–80, http://dx.doi.org/10.1108/13552540810862028.
[12] J.P. Thomas, J.F. Rodríguez, Modeling the Fracture Strength between Fused-Deposition Extruded Roads, Proceedings of the 11th Solid Freeform Fabrication Symposium, (2000).
[13] S. Hwang, E.I. Reyes, K.S. Moom, R.C. Rumpf, N.S. Kim, et al., J. Electron. Mater. 44 (3) (2015) 771–777, http://dx.doi.org/10.1007/s11664-014-3425-6.
[14] D. Drummer, S. Cifuentes-Cuéllar, D. Rietzel, Suitability of PLA TCP for fused deposition modeling, Rapid Prototyp. J. 18 (6) (2012) 500–507, http://dx.doi.org/10.1108/13552541211272045.
[15] X. Liu, S. Li, Z. Liu, X. Zheng, X. Chen, Z. Wang, An investigation on distortion of PLA thin-plate part in the FDM process, Int. J. Adv. Manuf. Technol. 79 (5–8) (2015) 1117–1126, http://dx.doi.org/10.1007/s00170-015-6893-9.
[16] Y. Zhang, Y. Chou, Three-dimensional finite element analysis simulations of the fused deposition modelling process, proceedings of the institution of mechanical engineers, Part B: J. Eng. Manuf. 220 (10) (2006) 1663–1671, http://dx.doi.org/10.1243/09544054JEM572.
[17] C. Kousiatza, N. Chatzidai, D. Karalekas, Temperature mapping of 3D printed polymer plates: experimental and numerical study, Sensors 17 (3) (2017) 456, http://dx.doi.org/10.3390/s17030456.
[18] C. Kousiatza, D. Karalekas, In-situ monitoring of strain and temperature distributions during fused deposition modeling process, Mater. Des. 97 (2016) 400–406, http://dx.doi.org/10.1016/j.matdes.2016.02.099.
[19] Q. Sun, G.M. Rizvi, C.T. Bellehumeur, Experimental Study of the Cooling Characteristics of Polymer Filaments in FDM and Impact on the Mesostructures and Properties of Prototypes, Solid Freeform Fabrication Symposium, Austin, (2003).
[20] S.F. Costa, F.M. Duarte, J.A. Covas, Towards modelling of free form extrusion: analytical solution of transient heat transfer, Int. J. Mater. Form. 1 (1) (2008) 703–706, http://dx.doi.org/10.1007/s12289-008-0312-9.
[21] Y. Zhou, T. Nyberg, G. Xiong, D. Liu, Temperature Analysis in the Fused Deposition Modeling Process, 2016 3rd International Conference on Information Science and Control Engineering (ICISCE). Beijing , China, (2016), http://dx.doi.org/10.1109/ICISCE.2016.150.
[22] L.B. Ji, T.R. Zhou, Finite element simulation of temperature field in fused deposition modeling, Adv. Mater. Res. 97–101 (2010) 2585–2588 (DOI: 10.4028/www.scientific.net/AMR.97-101.2585).
[23] S. Dabiri, S. Schmid, G. Tryggvason, Fully Resolved Numerical Simulations of Fused Deposition Modeling, ASME 2014 International Manufacturing Science and Engineering Conference Collocated With the JSME 2014 International Conference on Materials and Processing and the 42nd North American Manufacturing Research Conference. Detroit, USA, (2014), http://dx.doi.org/10.1115/MSEC2014-4107.
[24] S.F. Costa, F.M. Duarte, J.A. Covas, Estimation of filament temperature and adhesion development in fused deposition techniques, J. Mater. Process. Technol. 245 (2017) 167–179, http://dx.doi.org/10.1016/j.jmatprotec.2017.02.026.
[25] L.T. Sin, A.R. Rahmat, W.A. Rahman, Polylactic Acid: PLA Biopolymer Technology and Applications, William Andrew, 2012 (chapter 3).
[26] W. Wu, P. Geng, G. Li, D. Zhao, H. Zhang, J. Zhao, Influence of layer thickness and raster angle on the mechanical properties of 3D-printed PEEK and a comparative mechanical study between PEEK and ABS, Mater. 8 (9) (2015) 5834–5846, http://dx.doi.org/10.3390/ma8095271.
[27] V. Kishore, C. Ajinjeru, A. Nycz, B. Post, J. Lindahl, V. Kunc, C. Duty, Infrared preheating to improve interlayer strength of big area additive manufacturing (BAAM) components, Addit. Manuf. 14 (2017) 7–12, http://dx.doi.org/10.1016/j.addma.2016.11.008.
[28] M. Faes, E. Ferraris, D. Moens, Influence of inter-layer cooling time on the quasi-static properties of ABS components produced via fused deposition modelling, Procedia CIRP. 42 (2016) 748–753, http://dx.doi.org/10.1016/j.procir.2016.02.313.
[29] J. Du, Z. Wei, X. Wang, J. Wang, Z. Chen, An improved fused deposition modeling process for forming large-size thin-walled parts, J. Mater. Process. Technol. 234 (2016) 332–341, http://dx.doi.org/10.1016/j.jmatprotec.2016.04.005.
[30] D.F. Parker, Fields Flows and Waves: An Introduction to Continuum Models, Springer, 2003 (chapter 2).